Iranian Polymer Journal (2019) 28:259–269
https://doi.org/10.1007/s13726-019-00699-2

ORIGINAL RESEARCH

Mesopores variation in polyacrylonitrile fibers during dry-jet wet spinning process

Quan Gao[1,2] · Min Jing[3] · Chengguo Wang[1,2] · Meiling Chen[1,2] · Shengyao Zhao[1,2] · Wenli Wang[1,2] · Jianjie Qin[1,2]

Received: 28 September 2018 / Accepted: 10 March 2019 / Published online: 14 March 2019

Abstract

The mesopore structures in polyacrylonitrile (PAN) fibers during dry-jet wet spinning process were investigated by high-resolution transmission electron microscopy (HRTEM) and image analysis utilizing the ultrathin section technique. The morphologies and dimension distribution of the mesopores in the surface and core regions of the nascent fibers and PAN fibers are presented. All fibers exhibited lamellar-like structures perpendicular to the fiber axis and the mesopores were distributed between the lamellae. For nascent fibers, the size and volume of the mesopores increased with increasing air gap and decreased with increasing drawing ratio. In addition, the widths of the mesopores were larger than their lengths. Consequently, the size and content of the mesopores in nascent fibers could be adjusted by controlling coagulation conditions. During the post-spinning process, the size and volume of the mesopores in PAN fibers decreased efficiently by hot drawing in a hot water washing bath, in hot steam chambers or on hot rollers. Moreover, the lengths of the mesopores were larger than their widths. In all fiber samples, the number and size of the mesopores in the core region were larger than those in the surface region. In addition, the mechanical properties of fibers were correlated with dimension of the mesopores. Their tensile strength increased with decreasing mesopore widths and lengths.

Keywords PAN fiber · Nascent fiber · Mesopore · Ultrathin section · Mechanical properties

Introduction

Porosity is an intrinsic property of the polyacrylonitrile (PAN) fibers that is due to their microstructures and exists as voids (pores) between the lamellae, crystals and other elements of the fibers' texture [1, 2]. Their mechanical properties are largely limited by the presence of the pore defects where the stress accumulates, accelerating the formation and the development of cracks, which eventually results in catastrophic break [3, 4].

At present, there are many spinning techniques to make PAN precursor fibers, including wet spinning, dry spinning, and melt and electrospinning. However, to date, the dry spinning and melt spinning have yet not been reached the carbon fiber qualities by wet spinning, since they bring many defects into the fibers [5]. Meanwhile, in electrospinning, the fibers are short and are collected in the form of fiber mats rather than a continuous fiber filament [5, 6]. Therefore, the traditional wet spinning is the preferred technique for manufacturing carbon fiber precursors. Furthermore, to reduce the processing cost, the dry-jet wet spinning with high speed is developed to prepare high-quality precursor fibers [7]. During fiber formation and conversion process, the morphologies and size distribution of the pores in fibers were adjusted through controlling the spinning conditions [8]. Therefore, to decrease fiber porosity and increase fiber mechanical properties, it is important to study the evolution of pore structures and the relation between pores and mechanical properties during the dry-jet wet spinning process.

Electronic supplementary material The online version of this article (https://doi.org/10.1007/s13726-019-00699-2) contains supplementary material, which is available to authorized users.

✉ Chengguo Wang
wangchg@sdu.edu.cn

[1] Key Laboratory for Liquid-Solid Structural Evolution and Processing of Materials (Ministry of Education), Shandong University, Jinan 250061, China

[2] Carbon Fiber Engineering Research Center, School of Material Science and Engineering, Shandong University, Jinan 250061, China

[3] School of Material Science and Engineering, Shandong Jianzhu University, Jinan 250101, China

The pore structures in PAN fibers are originally formed in the coagulation bath during the spinning process [9]. The spinning dope solutions including dimethyl sulphoxide (DMSO) solvent and PAN were extruded into DMSO/H_2O coagulation bath and then became unstable thermodynamically due to counter diffusion phenomenon. Furthermore, the phase separation occurred and a polymer-rich phase formed the fiber skeletons, while a solvent-rich phase formed pores [10]. Therefore, the counter diffusion process was affected by variation in effective parameters of spinning dope and coagulation bath conditions, which had a significant influence on pore formation and growth [10, 11]. During post-spinning process, the DMSO solvent was gradually removed, resulting in shrinking of fiber skeletons and the partial collapsing of the pores [12]. Therefore, the pore development was controlled by drawing conditions.

In conclusion, there are two effective methods to improve the size and number of the voids and reduce the overall porosity of PAN fibers during the spinning process, namely preventing voids growth in the coagulation bath and healing the previously formed voids by hot drawing the nascent fibers [11, 13, 14]. Unfortunately, the pores are hard to eliminate completely. Therefore, the pore defects may still retain their geometrical identity through the manufacturing process and would generate into the final carbon fibers, which are thought to be responsible for the decrease in carbon fiber tensile strength [2, 15]. Accordingly, it is necessary to acquire more information on emerging pores during manufacturing process, thereby minimizing the porosity of the PAN precursor fibers through control of the spinning conditions.

The pore structures of the PAN fibers have been studied by several methods to estimate their parameters. The most common indirect methods including the classical absorption/desorption [16, 17], mercury porosimetry [1, 18], and thermoporometry [9, 12, 19] are frequently used, with their underlying principle including the effect of capillarity and fluid flow in the porous material or on the filtration effect [20], which only provide the dimension information. However, the most direct method of the electron microscopy makes it possible to reveal the shape and morphology of pores through the evaluations of the microscopic pictures of the fiber with image analysis.

Atomic force microscopy (AFM) can only focus on nanopores of the fiber surface [2], and the pores with relatively larger diameters distributed in the fiber surface and cross section are easily observed by scanning electron microscopy (SEM) [9, 11, 21, 22]. However, it is hard to obtain the morphology and information on the location of the pores in fiber's interior directly. In addition, the method of preparing the objects also restricts exploring the pores. To determine the fine structures, high-resolution transmission electron microscopy (HRTEM) is an indispensable method [23, 24] and the ultrathin section is also a sufficiently well technique for interior fine structure observation [23, 25].

According to the International Union of Pure and Applied Chemistry (IUPAC) recommendations, there are three kinds of pores dimensionally: micropore ($D < 2$ nm), mesopore (2 nm $< D <$ 50 nm) and macropore ($D > 50$ nm). The micropores in PAN fibers are considered as sufficiently compact, since the distance between the elements is very small [26]. However, mesopores that distinctly perturb the compactness and homogeneity of the PAN and carbon fibers have a negative effect on their mechanical properties and are difficult to observe by direct electron microscopy. Herein, longitudinal ultrathin sections of PAN fibers were prepared and the mesopore structures were characterized by HRTEM. In addition, the frequency histograms for mesopore sizes were also presented and analyzed. The effect of the coagulation conditions and hot-drawing conditions on the mesopore variation is discussed. A possible correlation between the mesopore structures of PAN fibers and their mechanical properties is proposed.

Experimental

Preparation of PAN fiber

The PAN copolymer was obtained through an aqueous polymerization in our laboratory. The acrylonitirle (AN, AR) and itaconic acid (IA, AR) in water were initiated by ammonium persulfate (APS, AR) to prepare the PAN copolymer (AN:IA = 98.5:1.5) with a viscosity molecular weight of approximately 1.5×10^5 g/mol (measured by the viscometry, as shown in Fig. S1, in Supplementary Materials), under the condition of nitrogen protection. Then, PAN powders were deposited on the bottom of the flask being the only component insoluble in water. Finally, the PAN powders and DMSO solvent with the mass ratio of 18.5:81.5 were mixed by the machine of a double-screw extruder, yielding the spinning solution dope.

The dry-jet wet spinning process was conducted on a pilot plant at Shandong University, China, as shown in Fig. 1. The spinning dope was extruded under the pressure through the spinneret (3000 orifices, $D = 0.12$ mm diameter) and passed through the coagulation bath (30 wt% DMSO solvent and 70 wt% water, 5 °C) to obtain the PAN nascent fibers designated as: *N*1, *N*2 and *N*3 samples. The parameters of these nascent fibers are listed in Table 1. The air gap distance for the nascent fibers *N*1, *N*2 and *N*3 were 3 mm, 8 mm and 3 mm, respectively, while the drawing ratio (defined as the ratio of the first roller take-up velocity V_1 to the dope extrusion velocity V_0) was set as 2.5, 2.5 and 3.8, respectively (keeping V_1 constant and different drawing ratios could be attained by changing V_0). Therefore, the time of the counter

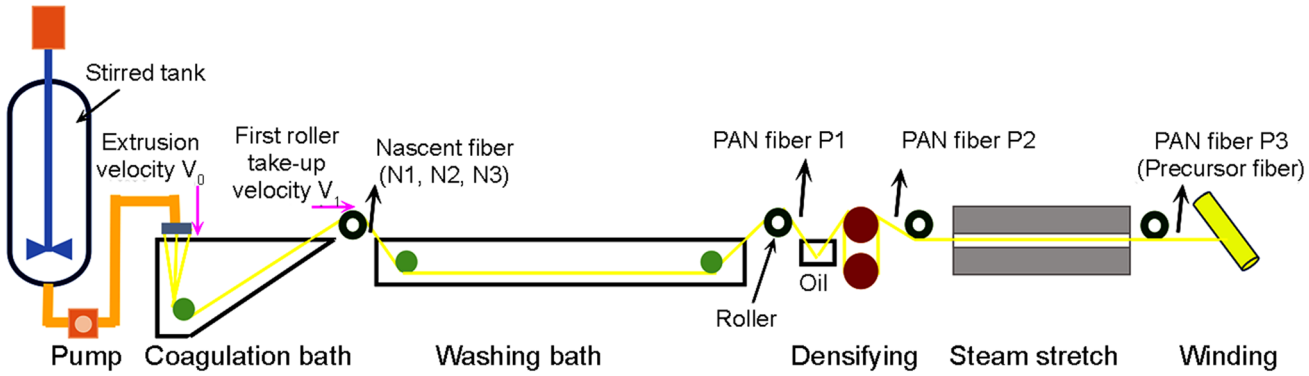

Fig. 1 Dry-jet wet spinning process and the PAN fiber samples collected point

Table 1 Parameters of the nascent fiber and sampling point of the PAN fiber

Nascent fiber obtained after coagulation process			PAN fiber during post-spinning process	
Sample	Air gap distance (mm)	Drawing ratio	Sample	Sampling point[a]
*N*1	3	2.5	*P*1	After washing bath
*N*2	8	2.5	*P*2	After densifying process
*N*3	3	3.8	*P*3	After steam stretching

[a]Sampling point of the PAN fiber as shown in Fig. 1

diffusion was the same in all nascent fibers. Then, the nascent fiber *N*3 was stretched in multi-steps in warm water with degrees of temperature (ranging from 45 to 80 °C) with a total drawing ratio of 2.9 to obtain PAN fiber *P*1. Moreover, the PAN fibers were immersed in oil for isolation and protection, and successively densified at 140 °C with a drawing ratio of 1 to obtain PAN fiber *P*2. Finally, the PAN fibers were stretched in water vapor with a drawing ratio of 3.5 to obtain PAN fiber *P*3 (precursor fiber). In order to assess the mesopore structures during the spinning process, some PAN fiber samples (nascent fibers *N*1–*N*3 and PAN fibers *P*1–*P*3) were collected (as shown in Fig. 1; Table 1) and treated further.

Preparation of the ultrathin section

The fiber object for HRTEM observation was prepared by an ultrathin sectioning technology. Firstly, some fibers were embedded and fixed by epoxy resin solution to prevent fiber sliding over cutting process. Following solidification, longitudinal ultrathin sections were cut through a diamond knife by an ultratome (LKB-2088, BROMMA Ltd., Sweden). The sections were controlled within 50 nm in thickness. Finally, the ultrathin sections were easy to float on the surface of purified water in the sink. To better support samples, copper grids with supported carbon film were used to collect ultrathin sections.

Characterization

The longitudinal ultrathin sections of PAN fiber samples were examined by HRTEM (JEM-2100, JEOL Ltd., Japan) at an acceleration voltage of 200 kV. The image processing technique was carried out to measure the pore size of the mesopore structures in fiber samples using the ImageJ software. According to the results given in Figs. S2 and S3 (ref to Supplementary Materials), only the thickness contrast made a contribution to the electronic imaging during characterizing the PAN fiber longitudinal ultrathin section by HRTEM. Therefore, the white region in HRTEM image was considered as the space of the mesopore structures in the fiber. The width (perpendicular to the fiber axis) and length (parallel to the fiber axis) of the mesopores were proposed in this paper to characterize the fiber size property. Furthermore, the pore size distribution was represented by a histogram describing the frequency of pore size:

$$\text{Frequency}\ (\%) = \text{number of pores with pore size}/\text{total number of pores}.$$

The frequency histogram pictures for width and length of the mesopores are also presented as analyzed by the Origin software.

The tensile strengths of fiber samples were determined by a monofilament tensile testing machine (XQ-1, Donghua University, China) at room temperature. During the measurement, the gauge length and stretching speed were chosen as 20 mm and 10 mm/min, respectively. A series of 10 single-fiber samples were carried out for the tensile test measurement.

Results and discussion

Mesopore in the PAN nascent fiber

Figure 2 shows the HRTEM morphology of the PAN nascent fiber longitudinal ultrathin section. The morphologies of surface region and core region of PAN fibers are presented in Fig. 2a–f, respectively, taken from a single fiber. All the HRTEM images show a lamella-like structure

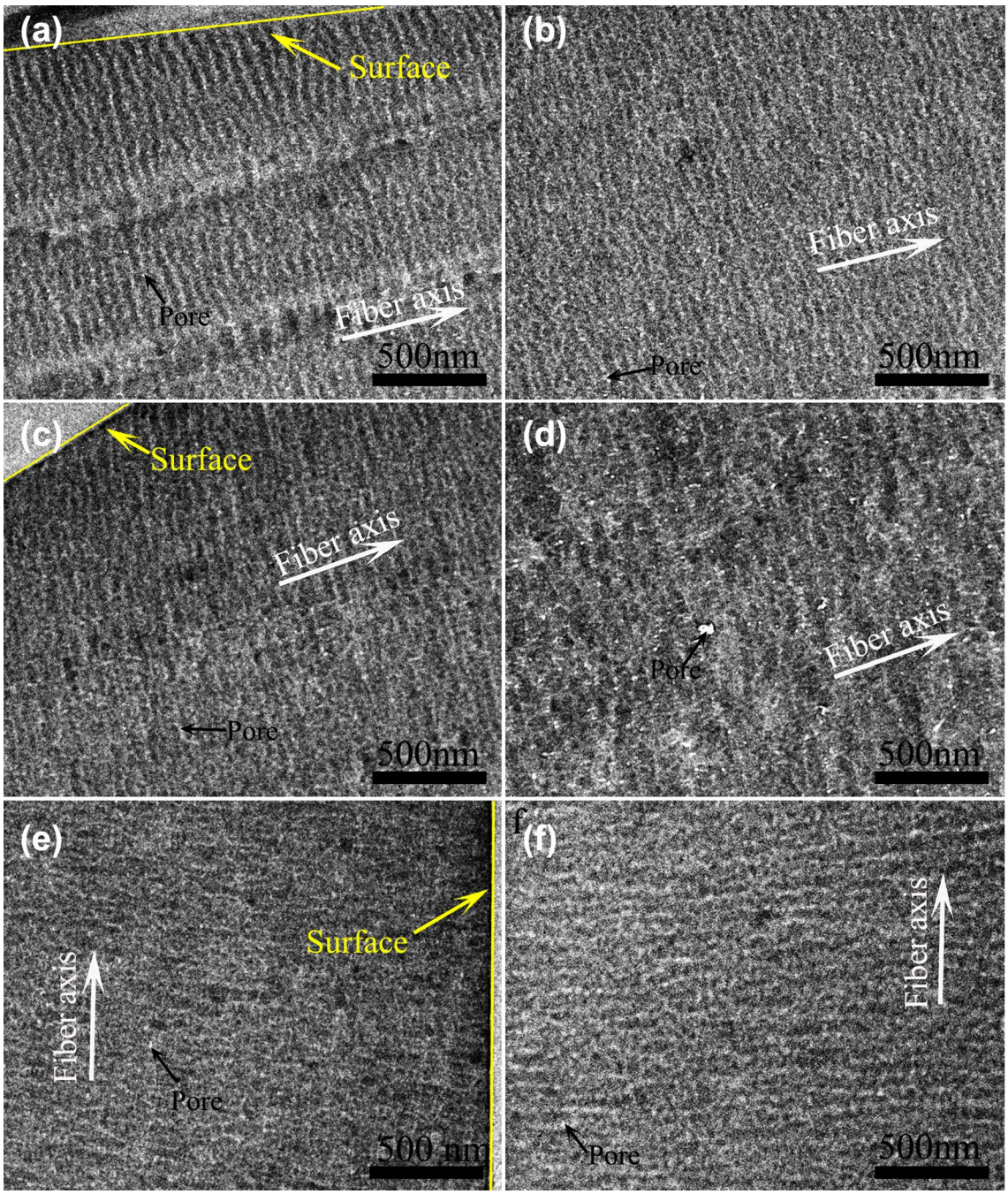

Fig. 2 HRTEM morphology of the PAN nascent fiber longitudinal ultrathin section **a, b** *N*1; **c, d** *N*2; and **e, f** *N*3

perpendicular to the fiber axis, formed by folded molecular chains during the coagulation process [27–29]. In addition, the mesopore structures are distributed between the lamellae.

Compared to wet spinning where fiber filaments were immersed directly in a coagulation bath followed by their instant coagulation, in dry-jet wet spinning process, a thin solidified skin (as shown in Fig. 2) was built to avoid sudden mass transfer by diffusion [30]. Meanwhile, the molecular orientation in nascent fiber induced by shear stress within the spinneret could be frozen into the wet-spun fiber but relax in a small air gap region for the dry-jet wet-spinning fiber [31]. During the coagulation process, a phase-separation occurred due to solvent/non-solvent exchange, which was restricted by a thin solidified skin. Meanwhile, the molecular chains were folded into the lamellae [29] and a poor-polymer phase was formed into the mesopores distributed between the lamellae. The mesopores might be considered as the path where DMSO solvent is diffused out along the fiber transverse direction. Consequently, the counter diffusion was promoted by not only the concentration gradient but also by the compression field in the transverse direction.

Figure 2a, b presents the lamellae in the nascent fiber *N*1. There are many mesopores between the lamellae and they have the relatively larger number and length in the core region than those in the surface region. On increasing the air gap, the more lamellae structures and oriented structures in the surface region were frozen due to significant solidification by cooling or gelation by moisture evaporation on fiber surface, which increased the thickness of the skin. Meanwhile, relaxing time also increases, which induces more oriented chains in the core region to relax.

Therefore, the lamellae in the surface region of the nascent fiber *N*2 (Fig. 2c) are packed more closely than that of *N*1, while the lamellae are arranged loosely and a large number of mesopores are distributed unevenly in the core region (Fig. 2d). Furthermore, compared to the nascent fiber *N*1, the morphological difference between the surface region and the core region became more obvious for the *N*2. The orientation and regularity of the molecular chains in *N*3 are improved by increasing the drawing ratio. As shown in Fig. 2e, f, the thickness of the lamellae in *N*3 is smaller than that in *N*1. Furthermore, the morphological difference between the surface region and core region of *N*3 is narrowed, and the number and size of the mesopores are decreased.

The dimensions of the mesopores perpendicular (width) and parallel (length) to the fiber axis were determined by measuring the linear distance of the white region in the respective direction. The histograms in Fig. 3 show the frequency distributions of width and length of the mesopores in the nascent fibers. The distributions of the mesopore length in the surface region are unimodal, but other distributions

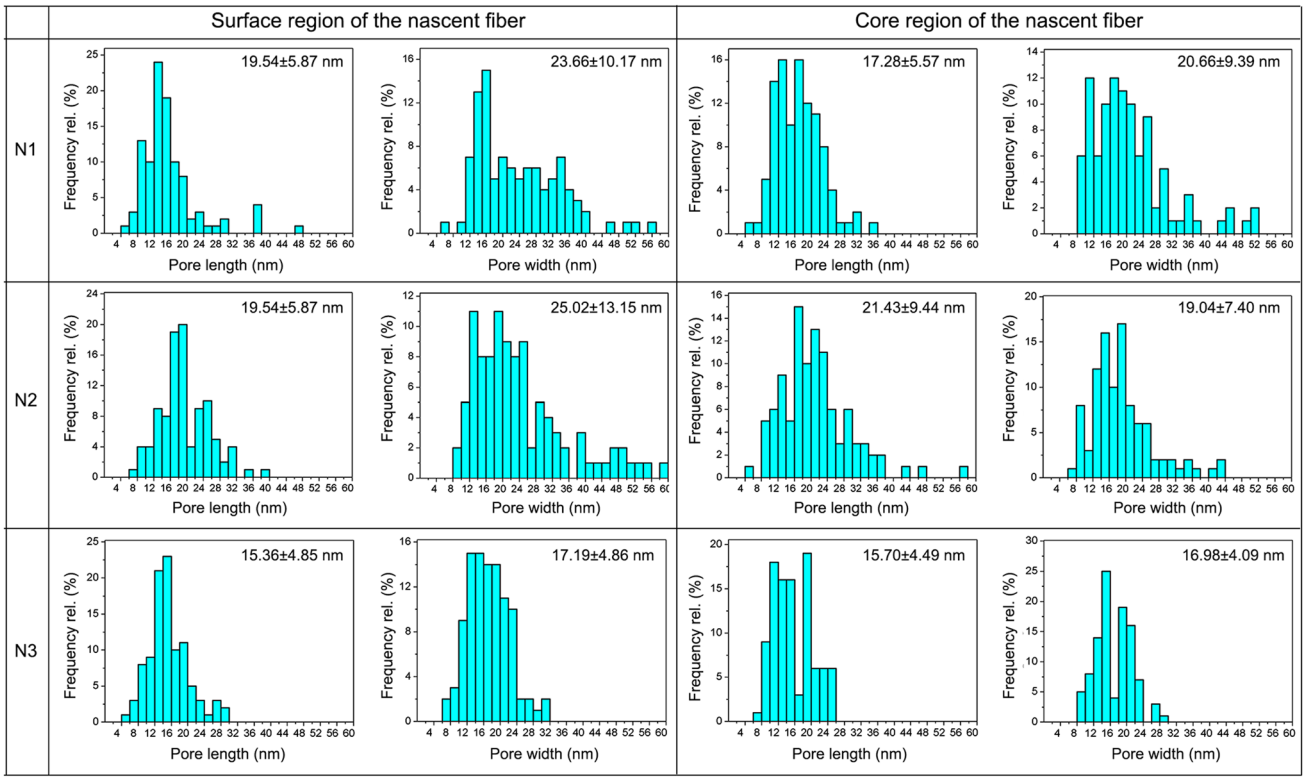

Fig. 3 Histograms of the size distribution of mesopores in nascent fiber

Table 2 Mesopores size of nascent fibers

Sample	Mean length $L \pm \sigma$ (nm)	Mean width $W \pm \sigma$ (nm)	α (L/W)	A_{eff}
*N*1 surface	15.56 ± 6.99	23.66 ± 10.17	0.66	368.15
*N*1 core	17.28 ± 5.57	20.66 ± 9.39	0.84	357.00
*N*2 surface	19.54 ± 5.87	25.02 ± 13.15	0.78	488.89
*N*2 core	21.43 ± 9.44	19.04 ± 7.40	1.13	408.03
*N*3 surface	15.36 ± 4.85	17.19 ± 4.86	0.89	264.04
*N*3 core	15.70 ± 4.49	16.98 ± 4.09	0.92	266.59

of the mesopores are multimodal. Compared with the nascent fiber *N*1, the length and width distribution are relatively broad in *N*2. Contrarily, the length and width distribution become narrow in *N*3 by increasing the drawing ratio.

The numerical values of mesopore width and length of the nascent fiber are given in Table 2 according to Figs. 2 and 3. In all nascent fibers, the mesopore length values in the core region are larger than those in the surface region, but the widths are complex. A significant difference in the shape of mesopores has appeared in the nascent fibers, in particular that of the aspect ratio (α = length/width). The aspect ratios of the mesopores of nascent fiber *N*1 are significantly small with $\alpha = 0.66$ and $\alpha = 0.84$, indicating that these mesopores belong to the linear channel pores and their major axes are perpendicular to the fiber axis. On increasing the air gap, the aspect ratios of the mesopores in the surface region and core region of the nascent fiber *N*2 are $\alpha = 0.78$ and $\alpha = 1.19$, respectively. Consequently, the relaxation of the oriented molecular chains in the long air gap may bring a huge effect on the shape of the mesopores. For the nascent fiber *N*3, the mesopores have an almost round shape with aspect ratios close to 1 and the mesopore sizes decrease apparently.

A measure of the mesopore area is the product of width and length, which is defined as effective mesopore area A_{eff} [2], and the effective mesopore area of fiber longitudinal ultrathin section can be used to represent fiber volume. The effective mesopore areas in the surface and core region of the nascent fibers *N*1, *N*2 and *N*3 amounted to A_{eff} = 368.15/357.00, A_{eff} = 488.89/382.95, and A_{eff} = 264.04/266.59, respectively. Compared to the nascent fiber *N*1, the mesopore volume of *N*2 is increased and the mesopore volume of *N*3 is decreased.

During coagulation process, the formation and growth of the mesopores were influenced by the variation in drawing ratio and air gap distance. By increasing the air gap, the diffusion of solvent and non-solvent was limited by increasing the skin thickness, which would bring unwanted influence on the mesopore structures, and the mesopore sizes and volume increased in *N*2. As for *N*3, a high drawing ratio helped alignment of the molecular chains and tended to push the solvent out and prevent the entry of the non-solvent into the core during the coagulation process [32]. Therefore, the diffusion of the solvent/non-solvent is decreased by increasing the drawing ratio, which could be attributed to the orientation of the voids along the fiber axis, the increase in dense ligament and the loss of connectivity between the voids (blocking transport channels of solvent and non-solvent) [10, 33, 34]. Thus, the sizes and volumes of the mesopores are decreased in nascent fiber *N*3.

Table 3 Mechanical properties of PAN nascent fibers

Nascent fiber	Titer/dtex	Strength		Tensile strength/ cNdtex^{-1}
		Average date/cN	CV[a]	
*N*1	15.8	8.94	11.4	0.57
*N*2	13.1	7.3	13.69	0.56
*N*3	7.38	5.76	8.83	0.78

[a]CV value is the ratio of the standard deviation of the tensile strength data to its average value

Mesopore structures/mechanical properties relation in PAN nascent fibers

The mechanical properties of the prepared PAN fibers are listed in Table 3. Due to relatively large titers of nascent fibers, nascent fibers *N*1, *N*2 and *N*3 have smaller tensile strength values [7, 35, 36]. There are no obvious grooves and cracks on the surface of nascent fiber, as shown in Fig. S4 (in Supplementary Materials). Thus, according to the Griffith's theory [37], the fiber tensile strength is mainly limited by the mesopore defects content, where the stress is accumulated and the crack is formed easily under load, resulting in fiber's catastrophic failure. Furthermore, the comparison of the mesopore dimension with mechanical properties of different nascent fiber samples reveals a clear correlation, as demonstrated in the correlation plot in Fig. 4. It shows that the tensile strength of the nascent fiber decreases with the increase in mesopore width and length. This lowering trend in tensile strength with increasing effective mesopore area may be caused by higher number of large defects and the breaking original fibers.

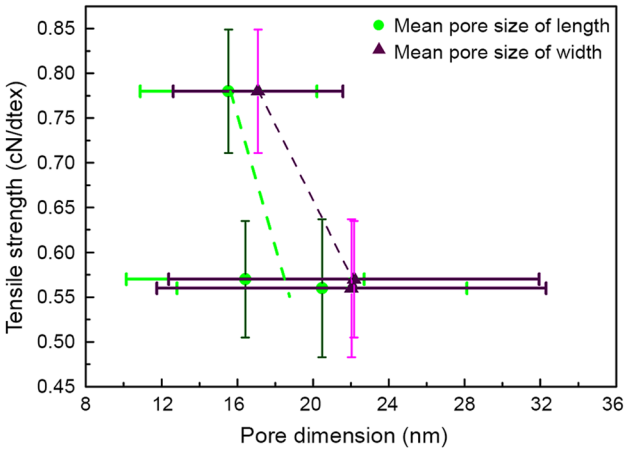

Fig. 4 Correlation between tensile strength and mesopore dimensions of the nascent fibers

Mesopore in the PAN fiber during spinning process

A large number of pore defects were existed in the nascent fibers, which were the main cause of the lowered tensile strength. Therefore, there was a chance to reduce the porosity of the PAN fibers through hot drawing at various stages of the post-spinning process, such as drawing in hot water washing bath, in hot steam chambers or on the hot rollers [5, 13, 22]. However, drawability of the PAN fibers during the post-spinning process was determined by the size distribution and number of the mesopores and interior microstructure morphologies of the nascent fibers. Consequently, the nascent fiber *N*3 was chosen to prepare the PAN precursor fibers, experienced the process of washing, densifying and steam stretching.

Figure 5 shows HRTEM morphology of the PAN fiber longitudinal ultrathin section. Compared to the nascent fibers, the lamellae are packed more closely in the surface region but there is still a great deal of mesopores in fiber *P*1 (Fig. 5a, b), resulting in DMSO removed and relaxing the lamellae ordered structures in the washing bath. The mesopores with oval shapes are oriented along the fiber axis under the stretching field. After densification treatment, the mesopores have been collapsed and merged. Consequently, the number and size of the mesopores have decreased in fiber *P*2 (Fig. 5c, d), but there is still a part of interior water failed to eliminate due to the dense skin, and some mesopores being merged to form a few macropores in the core region. After steam stretching, the lamellae are packed more closely in the fiber *P*3 (Fig. 5e, f) and the number and size of the mesopores are decreased.

The histograms in Fig. 6 show the frequency distributions of width and length of the mesopores in the PAN fibers. The center of the length and width distribution is moved into smaller size during the spinning process. The histograms of the length and width of the mesopores show a symmetric frequency distribution, which may be caused by a small number of the mesopores with large sizes. Their length and width in the core region are larger than those in the surface region. In addition, there are some macropores in the core region of PAN fibers *P*1 and *P*2. Consequently, the size distribution of the mesopores shifts toward smaller values through closely arranged lamellae during hot-drawing process.

The numerical values of the mesopore width and length of the PAN fiber are given in Table 4 according to Figs. 5 and 6. Apparently, the lengths of the mesopores in the PAN fiber are larger than their widths, and the mesopores have the oval shape with an aspect ratio > 1, oriented along the fiber axis. These results are attributed to the stretching field during post-spinning processing. The effective mesopore areas of the PAN fibers *P*1, *P*2 and *P*3 have amounted to A_{eff} = 193.42/ 298.87, A_{eff} = 133.09/262.22, and A_{eff} = 40.85/181.16, respectively. Compared with the nascent fiber *N*3, the mesopore volume of PAN fibers is decreased successively during the post-spinning process.

After coagulation process, the nascent fibers have been washed to remove residual solvent using warm water and led to high diffusion of water into the fiber, which could cause large voids. To prevent the formation and development of a large number of the mesopores in the washing bath, the several washing baths in different gradient temperatures were used to avoid rapid influx of water [5]. Furthermore, the use of drawing enhanced the axial orientation of the molecular chains and fiber linear density to decrease the mesopore volume. The mesopores in the washing steps were stretched along the fiber axis. Consequently, compared with the nascent fiber *N*3, A_{eff} in the surface region was decreased and A_{eff} in the core region increased instead in the PAN fiber *P*1, but obviously their aspect ratio has been increased. During the densification process, wet fibers were treated on the hot rollers with roller temperature being greater than the glass transition temperature of PAN fibers. Therefore, the water in pores was desorbed from the wet fibers, which led to the collapse of the mesopores. Consequently, the mesopore sizes decreased in the PAN fiber *P*2 and the A_{ff} in the surface region and core region decreased by 31.2% and 12.2%, respectively. During the saturated steam stretching process, the water steam serving as a plasticizer could reduce the Van der Waals force between the molecular chains at high pressure and temperature condition, which could improve the molecular orientation along the fiber axis and decreased the size and volume of the mesopores [38]. Therefore, the mesopore sizes decreased obviously in PAN fiber *P*3 and A_{ff} in the surface region and core region by 69.3% and 30.9%, respectively. Consequently, the steam stretching was more effective in reducing the size and volume of the mesopores in PAN fibers in comparison with their drawing in washing bath and densification process.

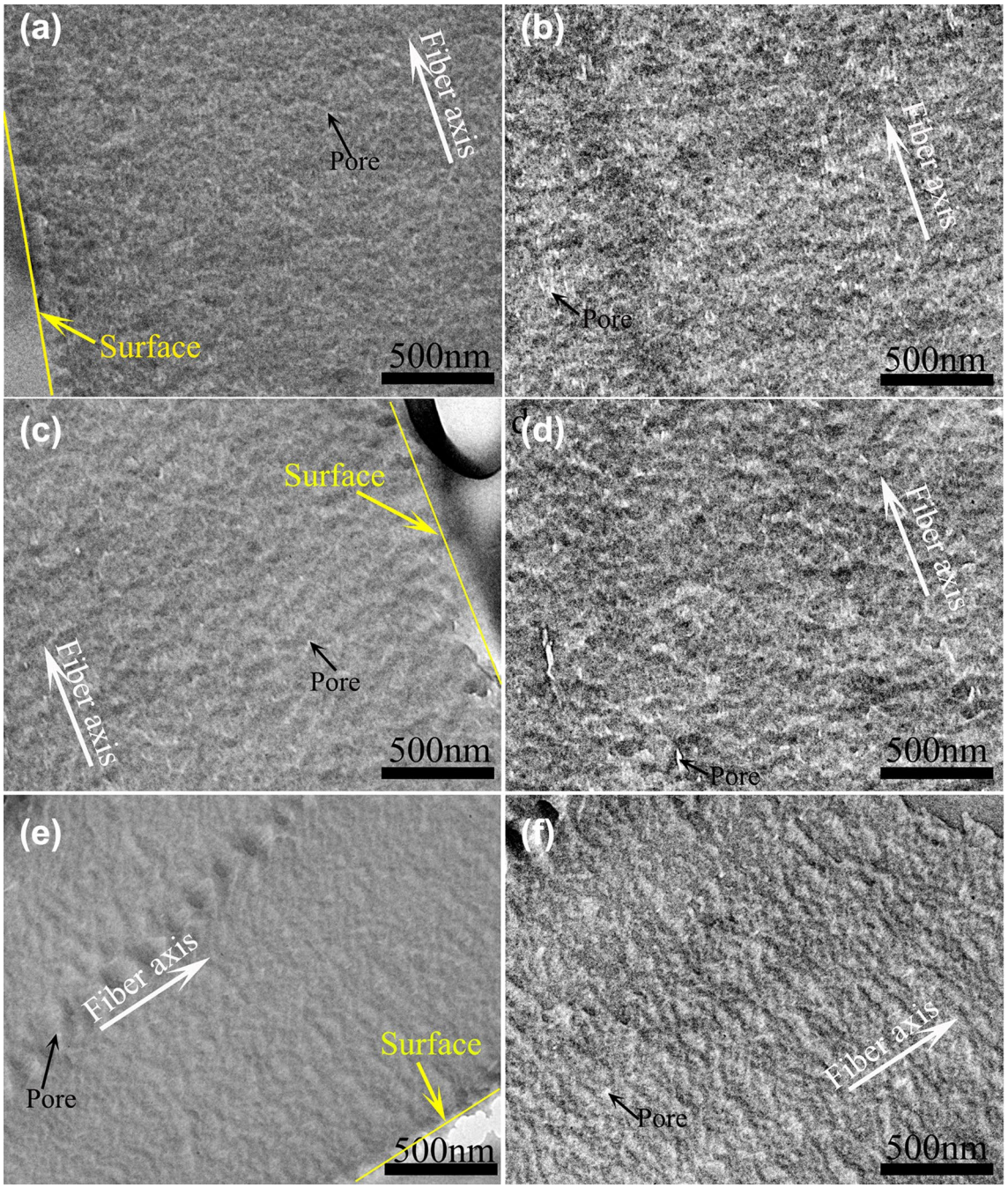

Fig. 5 HRTEM morphology of the PAN fiber longitudinal ultrathin section **a, b** *P*1; **c, d** *P*2; and **e, f** *P*3

Correlation between mesopore structure and mechanical properties of PAN fiber

The mechanical properties of the PAN fibers are listed in Table 5. During the post-spinning process, the titers of the PAN fibers decrease (Titer: $P1 > P2 > P3$) and their tensile strengths increase (tensile strength: $P1 < P2 < P3$). Consequently, the hot drawing can efficiently improve the tensile strength of the PAN fibers. As shown in Fig. S5 (in Supplementary Materials), the surfaces are smooth and there are no obvious grooves and cracks for PAN fibers. So, decreasing the content and sizes of the mesopore defects is one of the most efficient ways to enhance the tensile strength of the PAN fibers from the point of the material defects [39]. Comparison of the mesopore dimension with mechanical properties of different PAN fibers reveals a clear correlation, as demonstrated in the correlation plot in Fig. 7. It shows that the tensile strength of the PAN fibers increases with decreasing

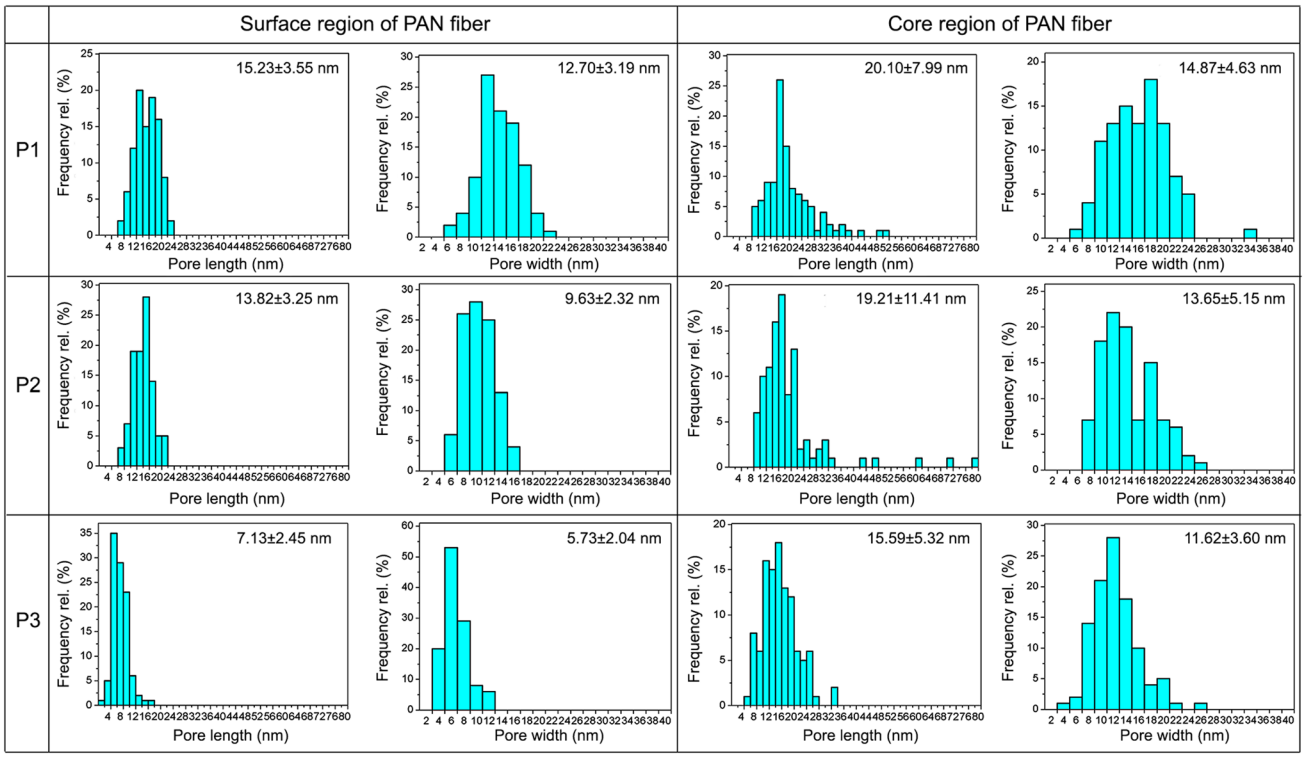

Fig. 6 Histograms of the size distribution of the mesopores in PAN fiber

Table 4 Mesopores size of PAN fiber

Sample	Mean length $L \pm \sigma$ (nm)	Mean width $W \pm \sigma$ (nm)	α (L/W)	A_{eff}
*P*1-surface	15.23 ± 3.55	12.70 ± 3.19	1.20	193.42
*P*1-core	20.10 ± 7.99	14.87 ± 4.63	1.35	298.87
*P*2-surface	13.82 ± 3.25	9.63 ± 2.32	1.44	133.09
*P*2-core	19.21 ± 11.41	13.65 ± 5.15	1.41	262.22
*P*3-surface	7.13 ± 2.45	5.73 ± 2.04	1.24	40.85
*P*3-core	15.59 ± 5.32	11.62 ± 3.60	1.34	181.16

Table 5 Mechanical properties of the PAN fibers

PAN fiber	Titer/dtex	Strength		Tensile strength/ cNdtex^{-1}
		Average date/cN	CV[a]	
*P*1	2.26	6.70	7.13	2.96
*P*2	1.77	6.25	5.44	3.53
*P*3	0.53	4.53	19.83	8.55

[a]CV value is the ratio of the standard deviation of the tensile strength data to its average value

mesopores width and length. Consequently, the content of the mesopores decreases by the hot drawing during the post-spinning process, which can improve the tensile strength of the PAN fibers.

Conclusion

The mesopore variations in PAN fibers during the dry-jet spinning process were investigated. The mesopores were mainly distributed between the lamellae in the PAN fibers. The mesopore sizes and volume of the nascent fibers increased with increasing the air gap and decreased with increasing the drawing ratio. Their widths were larger than their lengths. Then, the size and volume of the mesopores decreased through hot drawing during the post-spinning process. Their lengths were larger than their widths, which indicated that the mesopores were oriented along the fiber axis under the stretching field. The mesopore sizes and their amount in the core region were larger than those in the surface region, indicating that the denser surfaced

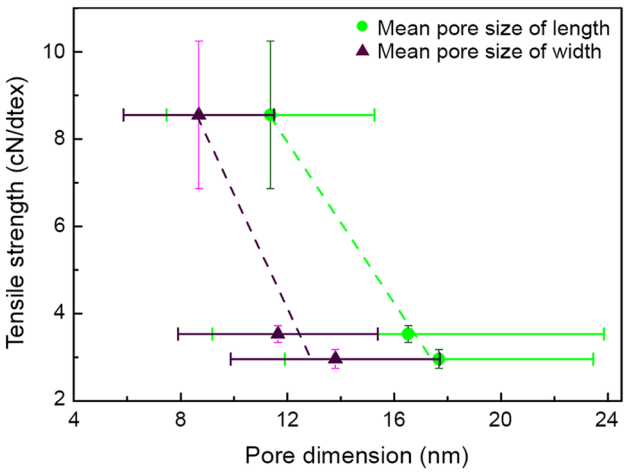

Fig. 7 Correlation between tensile strength and mesopore dimensions of the PAN fibers

structures and loose core part were coexisted in PAN fiber, termed as "skin-core" structures. Due to the relatively large titer of the nascent fibers, they had smaller tensile strengths. The tensile strength of the PAN fiber samples increased during the post-spinning process. The mechanical properties of the PAN fibers were correlated with the dimension of the mesopores. The fiber tensile strength increased with decreasing the mesopore width and length for the nascent fiber and PAN fibers.

Acknowledgements This work was supported by the National Natural Science Foundation, China (Grant nos. 51773110 and 51573087) and the Natural Science Foundation of Shandong Province, China (Grant nos. ZR2016EMM16 and ZR2018BEM036).

References

1. Tsai JS (1994) The traps in characterisation of PAN and carbon fibers by the mercury porosimetry method. J Polym Res 1:393–397
2. Kunzmann C, Moosburger-Will J, Horn S (2016) High-resolution imaging of the nanostructured surface of polyacrylonitrile-based fibers. J Mater Sci 51:1–11
3. Schaper A, Zenke D, Schulz E, Hirte R, Taege M (1989) Structure-property relationships of high-performance polyethylene fibres. Phys Status Solidi A 116:179–195
4. Watt W (1972) Carbon work at the royal aircraft establishment. Carbon 10:121–143
5. Kaur J, Millington K, Smith S (2016) Producing high-quality precursor polymer and fibers to achieve theoretical strength in carbon fibers: a review. J Appl Polym Sci 133:43963
6. Heseltine PL, Ahmed J, Edirisinghe M (2018) Developments in pressurized gyration for the mass production of polymeric fibers. Macromol Mater Eng 303:1800218–1800231
7. Gao Q, Jing M, Wang C, Zhao S, Chen M, Qin J (2019) Preparation of high-quality polyacrylonitrile precursors for carbon fibers through a high drawing ratio in the coagulation bath during a dry-jet wet spinning process. J Macromol Sci B 58:128–140
8. Ghodsi A, Fashandi H, Zarrebini M, Mirzaei M (2018) Controlling the morphology of pvdf hollow fiber membranes by promotion of liquid-liquid phase separation. Adv Eng Mater 20:10
9. Sobhanipour P, Cheraghi R, Volinsky AA (2011) Thermoporometry study of coagulation bath temperature effect on polyacrylonitrile fibers morphology. Thermochim Acta 518:101–106
10. Arbab S, Noorpanah P, Mohammadi N, Soleimani M (2008) Designing index of void structure and tensile properties in wet-spun polyacrylonitrile (PAN) fiber. I. effect of dope polymer or nonsolvent concentration. J Appl Polym Sci 109:3461–3469
11. Arbab S, Mohammadi N, Noorpanah P (2008) Designing index of void structure and tensile modulus in wet-spun poly(acrylonitrile) proto-fibres. Part II: synergistic effect of dope non-solvent concentration and jet draw ratio. Iran Polym J 17:227–235
12. Hao J, Lu C, Zhou P, Li D (2013) Pore structure development of polyacrylonitrile nascent fibers in water stretching process. Thermochim Acta 569:42–47
13. Arbab S, Noorpanah P, Mohammadi N, Zeinolebadi A (2011) Simultaneous effects of polymer concentration, jet-stretching, and hot-drawing on microstructural development of wet-spun poly(acrylonitrile) fibers. Polym Bull 66:1267–1280
14. Arbab S, Mohammadi N, Noorpanah P (2008) The synergistic effect of dope concentration and jet-drawing on structure development of wet-spun poly(acrylonitrile). e-Polymers 80:1–11
15. Zhao Y, Yang Z, Fan W, Wang Y, Li G, Cong H, Yuan H (2018) Carbon nanotube/carbon fiber electrodes via chemical vapor deposition for simultaneous determination of ascorbic acid, dopamine and uric acid. Arab J Chem. https://doi.org/10.1016/j.arabjc.2018.11.002
16. Mahalingam S, Wu X, Edirisinghe M (2017) Evolution of self-generating porous microstructures in polyacrylonitrile-cellulose acetate blend fibres. Mater Design 134:259–271
17. Kim DH, Kim BH, Yang KS, Bang YH, Kim SR, Im HK (2011) Analysis of the microstructure and oxidation behavior of some commercial carbon fibers. J Korean Chem Soc 55:819–823
18. Fan J, Wen Y, Yang Y, Lang L (2009) Effect of air gap on morphology of polyacrylonitrile triangular fiber. Text Res J 79:611–617
19. Ishikiriyama K, Sakamoto A, Todoki M, Tayama T, Tanaka K, Kobayashi T (1995) Pore size distribution measurements of polymer hydrogel membranes for artificial kidneys using differential scanning calorimetry. Thermochim Acta 267:169–180
20. Neckář B, Ibrahim S (2003) Theoretical approach for determining pore characteristics between fibers. Text Res J 73:611–619
21. WangF WangS (2010) Characterization on pore size of honeycomb-patterned micro-porous PET fibers using image processing techniques. Ind Text 61:66–69
22. Arbab S, Noorpanah P, Mohammadi N, Zeinolebadi A (2011) Exploring the effects of non-solvent concentration, jet-stretching and hot-drawing on microstructure formation of poly(acrylonitrile) fibers during wet-spinning. J Polym Res 18:1343–1351
23. Zhou G, Byun JH, Lee SB, Yi JW, Lee W, Lee SK, Kim BS, Park JK, Lee SG, He L (2014) Nano structural analysis on stiffening phenomena of PAN-based carbon fibers during tensile deformation. Carbon 76:232–239
24. Guo X, Cheng Y, Fan Z, Feng Z, He LL, Liu R, Xu J (2016) New insights into orientation distribution of high strength polyacrylonitrile-based carbon fibers with skin-core structure. Carbon 109:444–452
25. Nebesářová J, Hozák P, Frank L, Štěpan P, Vancová M (2016) The cutting of ultrathin sections with the thickness less than 20 nm from biological specimens embedded in resin blocks. Microsc Res Tech 79:512–517
26. Zlatoustova LA, Smirnova VN, Medvedev VA, Serkov AT (2002) The Macroporosity of Polyacrylonitrile Fibre. Fibre Chem 34:200–202

27. Wang Q, Wang C, Bai Y, Yu M, Wang Y, Zhu B, Jing M, Ma J, Hu X, Zhao Y (2010) Fibrils separated from polyacrylonitrile fiber by ultrasonic etching in dimethylsulphoxide solution. J Polym Sci Pol Phys 48:617–619
28. Chen SS, Herms J Jr, Uhlmann LHP DR (1981) Oxidative stabilization of acrylic fibres. J Mater Sci 16:1490–1510
29. Gao Q, Jing M, Chen ML, Wang CG, Zhao SY, Qin JJ (2018) Research on pan nascent fiber interior microstructure through ultrasonic etching and ultrathin sectioning. Polym Sci Ser A 60:594–598
30. Shin KA, Park S, Nguyen HTB, Lee JH, Lee S, Joh HI, Jo SM (2018) Investigation into the gelation of polyacrylonitrile solution induced by dry-jet in spinning process and its effects on diffusional process in coagulation and structural properties of carbon fibers. Macromol Res 26:544–551
31. Qin JJ, Gu J, Chung TS (2001) Effect of wet and dry-jet wet spinning on the sheer-induced orientation during the formation of ultrafiltration hollow fiber membranes. J Membr Sci 182:57–75
32. Rahman MA, Ismail AF, Mustafa A (2007) The effect of residence time on the physical characteristics of PAN-based fibers produced using a solvent-free coagulation process. Mater Sci Eng A 448:275–280
33. Hou C, Liang Y, Wang CG (2005) Determination of the diffusion coefficient of H2O in polyacrylonitrile fiber formation. J Polym Res 12:49–52
34. Hou C, Qu RJ, Wang CH, Ying L (2006) Diffusion coefficient of DMF in acrylic fiber formation. J Appl Polym Sci 101:3616–3619
35. Ouyang Q, Chen YS, Wang XF, Ma HB, Li DH, Yang JX (2015) Supramolecular structure of highly oriented wet-spun polyacrylonitrile fibers used in the preparation of high-performance carbon fibers. J Polym Res 22:10
36. Gao Q, Jing M, Wang C, Chen M, Zhao S, Wang W, Qin J (2019) Correlation between fibril structures and mechanical properties of polyacrylonitrile fibers during the dry-jet wet spinning process. J Appl Polym Sci 136:47336
37. Schaper A, Zenke D, Schulz E, Hirte R, Taege M (1989) Structure-property relationships of high-performance polyethylene fibres. Phys Status Solidi Appl Res 116:179–195
38. Qin XY, Lu YG, Xiao H, Zhao WZ (2013) Effect of heating and stretching polyacrylonitrile precursor fibers in steam on the properties of stabilized fibers and carbon fibers. Polym Eng Sci 53:827–832
39. Doroudiani S, Kortschot MT (2003) Polystyrene foams. III. Structure-tensile properties relationships. J Appl Polym Sci 90:1427–1434